Energy Barriers to Rotation in Axially Chiral Analogues of 4-(Dimethylamino)pyridine

Alan C. Spivey,*[,†] Patrick Charbonneau,[‡] Tomasz Fekner,[†,§] Detlev H. Hochmuth,[∥] Adrian Maddaford,[†] Cecile Malardier-Jugroot,[‡] Alison J. Redgrave,[⊥] and Michael A. Whitehead[‡]

Department of Chemistry, University of Sheffield, Brook Hill, Sheffield S3 7HF, U.K., Theoretical Chemistry Laboratory, Department of Chemistry, McGill University, 801 Sherbrooke Street West, Montreal, Quebec, Canada H3A 2K6, Institut für Organische Chemie, Universität Hamburg, Martin-Luther-King-Platz 6, 20146 Hamburg, Germany, and GlaxoSmithKline Medicines Research Centre, Gunnels Wood Road, Stevenage, Hertfordshire SG1 2NY, U.K.

a.c.spivey@sheffield.ac.uk

Received February 26, 2001

The barriers to enantiomerization of a series of axially chiral biaryl analogues of 4-(dimethylamino)-pyridine (DMAP) **1**−**10** were determined experimentally by means of dynamic HPLC measurements and racemization studies. The barriers to rotation in derivatives **1**−**6** (based on the bicyclic 5-azaindoline core) were lower than those in the corresponding derivatives **7**−**10** (based on the monocyclic DMAP core). Semiempirical (PM3), ab initio Hartree−Fock (HF/STO-3G), and density functional theory (DFT/B3LYP/6-31G*) calculations reveal that these differences in barriers to rotation are the result of differing degrees of hybridization of the non-pyridyl nitrogen in the enantiomerization transition states (TSs). The importance of heteroatom hybridization as a factor in determining nonsteric contributions to barriers to rotation in azabiaryls of this type is discussed.

Introduction

We have recently described the synthesis of a novel series of axially chiral biaryl analogues (**II** and **III**) of the highly nucleophilic acylation catalyst 4-(dimethylamino)pyridine (DMAP) **I**. We have also shown that certain analogues, having sufficiently high barriers to rotation about the biaryl axis for their atropisomers to be configurationally stable, can be used in an enantiomerically pure form as catalysts for the efficient kinetic resolution of secondary alcohols.[2−5] During the development of these chiral catalysts, our initial studies focused on 7-aryl derivatives of 1-methyl-2-pyrrolino[3,2-*c*]pyridine (*N*-methyl-5-azaindoline) **II** as we anticipated that this bicyclic core unit would impart a higher resistance to rotation about the biaryl axis relative to the DMAP[6] core in analogous 3-aryl-DMAP derivatives **III**.[3] However, this turned out not to be the case: at ambient temperature, the 3-aryl-DMAP derivatives exhibit higher barriers to biaryl rotation than the corresponding *N*-methyl-5-azaindoline derivatives.[3,7] Here, we correlate the experimentally determined rotational barriers obtained by computer simulation of dynamic enantioselective HPLC chromatograms and from Eyring plots of racemization data with theoretical rotational barriers obtained by semiempirical (PM3), ab initio Hartree−Fock (HF/STO-3G), and density functional theory (DFT/B3LYP/6-31G*) methods for both series. Analysis of the data allows rationalization of the experimentally determined rotational barriers and prediction of barriers for compounds for which experimental data could not be obtained.

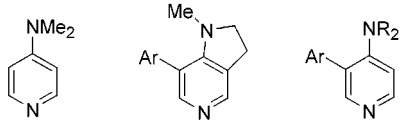

I II III

Results and Discussion

The experimentally determined barriers to rotation ($\Delta G^{\#}$) about the biaryl axis of DMAP derivatives **1**−**10** are shown in Figure 1. The barriers for configurationally labile derivatives **1**−**3**, **7**, and **8**[8] were determined by computer simulation of dynamic enantioselective HPLC

* To whom correspondence should be addressed. Tel: +44(0)114 22-29467. Fax: +44(0)114 27-38673. E-mail: a.c.spivey@sheffield.ac.uk.
† University of Sheffield.
‡ McGill University.
§ Present address: Department of Chemistry, The Ohio State University, 100 West 18th Ave., Columbus, OH 43210.
∥ Universität Hamburg.
⊥ GlaxoSmithKline Medicines Research Centre.

(1) Enantiomerization refers to the reversible microscopic interconversion of enantiomers with a rate constant k_{enant}. Racemization refers to the irreversible macroscopic conversion of an optically active mixture of enantiomers into or toward the racemate with a rate constant k_{racem} where $k_{racem} = 2k_{enant}$ since the interconversion of one molecule reduces the enantiomeric excess (ee) by two molecules. Dynamic HPLC studies and PM3, HF/STO-3G, and DFT/B3LYP/6-31G* calculations give k_{enant} directly, whereas Eyring plots give k_{racem} directly. Consequently, a statistical correction factor of 0.5 has been applied to the Eyring rate data to obtain correct kinetic parameters for enantiomerization (see Supporting Information).

(2) Spivey, A. C.; Fekner, T.; Adams, H. *Tetrahedron Lett.* **1998**, *39*, 8919−8922.
(3) Spivey, A. C.; Fekner, T.; Spey, S. E.; Adams, H. *J. Org. Chem.* **1999**, *64*, 9430−9443.
(4) Spivey, A. C.; Fekner, T.; Spey, S. E. *J. Org. Chem.* **2000**, *65*, 3154−3159.
(5) Spivey, A. C.; Maddaford, A.; Redgrave, A. *Org. Prep. Proced. Int.* **2000**, *32*, 331−365.

(6) The acronym DMAP is used here for all monocyclic 4-(di*alkyl*amino)pyridine-based structures, not just 4-(di*methyl*amino)pyridine.
(7) In an enantiomerically pure form, DMAP derivatives also impart significantly higher levels of stereoinduction in KR experiments than their *N*-methyl-5-azaindoline analogues (see ref 4).

10.1021/jo015593q CCC: $20.00
Published on Web 10/10/2001

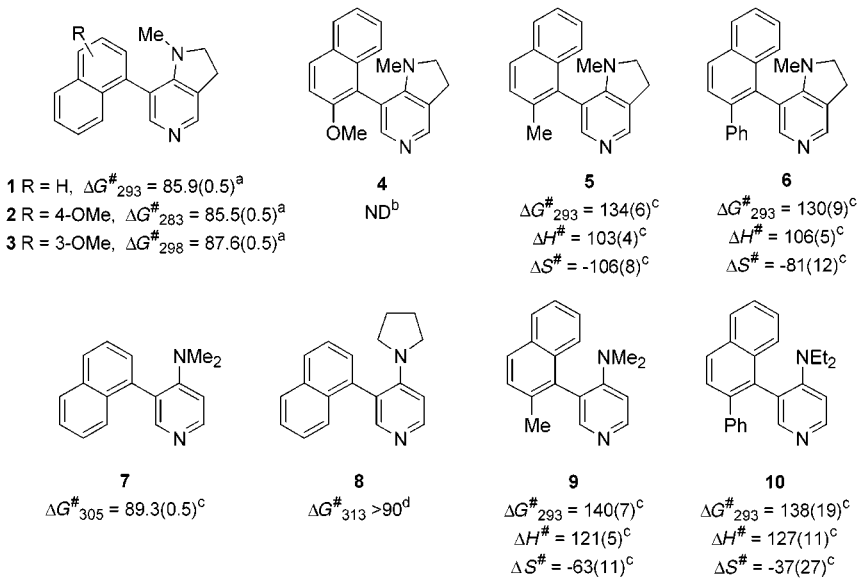

1 R = H, $\Delta G^{\#}_{293}$ = 85.9(0.5)[a]
2 R = 4-OMe, $\Delta G^{\#}_{283}$ = 85.5(0.5)[a]
3 R = 3-OMe, $\Delta G^{\#}_{298}$ = 87.6(0.5)[a]

4
ND[b]

5
$\Delta G^{\#}_{293}$ = 134(6)[c]
$\Delta H^{\#}$ = 103(4)[c]
$\Delta S^{\#}$ = -106(8)[c]

6
$\Delta G^{\#}_{293}$ = 130(9)[c]
$\Delta H^{\#}$ = 106(5)[c]
$\Delta S^{\#}$ = -81(12)[c]

7
$\Delta G^{\#}_{305}$ = 89.3(0.5)[c]

8
$\Delta G^{\#}_{313}$ >90[d]

9
$\Delta G^{\#}_{293}$ = 140(7)[c]
$\Delta H^{\#}$ = 121(5)[c]
$\Delta S^{\#}$ = -63(11)[c]

10
$\Delta G^{\#}_{293}$ = 138(19)[c]
$\Delta H^{\#}$ = 127(11)[c]
$\Delta S^{\#}$ = -37(27)[c]

Figure 1. Experimentally determined barriers to rotation ($\Delta G^{\#}$ (kJ/mol)) and associated kinetic parameters ($\Delta H^{\#}$ (kJ/mol) and $\Delta S^{\#}$ (J mol^{-1} K^{-1})) for enantiomerization.[1] Key: (a) obtained from a computer simulation of dynamic HPLC profiles; (b) values not determined, atropisomers inseparable on chiral HPLC (see text); (c) obtained from Eyring plots of racemization data;[1] (d) a lower limit, the plateau between atropisomers by chiral HPLC too low to simulate.

elution profiles.[9] We were unable to determine the value of $\Delta G^{\#}$ for biaryl **4** because we could not achieve good separation of its atropisomers by enantioselective HPLC.[10] The kinetic parameters for enantiomerization[1] of configurationally stable derivatives **5**, **6**, **9**, and **10** were determined from Eyring plots for the racemization[1] of individual enantiomers in sealed tubes in benzene in the temperature range 100−180 °C.

The trend in $\Delta G^{\#}$ values along the 5-azaindoline series shows, as expected, that tri-*ortho*-substituted biaryls **5** and **6** have significantly higher $\Delta G^{\#}$ values than di-*ortho*-substituted biaryls **1**−**3**. We expected biaryl **4** to display an intermediate value of $\Delta G^{\#}$ because, although it is tri-*ortho* substituted, *o*-alkoxy substituents are known to be less effective at hindering biphenyl rotation than carbon-based substituents.[11] However, our inability to resolve the atropisomers of this compound by enantioselective HPLC, combined with the unusual appearance of its ^{1}H NMR spectrum[10] and the knowledge that a number of biaryl systems comprising pyridyl rings display anomalously low barriers to rotation,[12] encouraged us to prepare biaryls **2** and **3**. We reasoned that if 2-methoxy-1-naphthyl biaryl **4** displayed a low barrier to rotation as the result of conjugation across the biaryl bond, then so too would 4-methoxy-1-naphthyl biaryl **2**, but not 3-methoxy-1-naphthyl biaryl **3**.[13,14] The fact that both these biaryls have almost identical values of $\Delta G^{\#}$ proves that any such conjugation is negligible but does not provide a guide to the value of $\Delta G^{\#}$ for biaryl **4**. We were particularly interested in knowing whether derivatives such as biaryl **4** were configurationally stable because these are intermediates en route to derivatives such as **5** and **6**, which we required for testing as chiral catalysts. Thus, preparative separation of the enantiomers of biaryl **4** could[15] provide access to a wide range of such catalyst candidates in an enantiomerically pure form without the need for time-consuming resolution of each derivative individually. This was our first motivation for the computational studies described below.

The second motivation was our finding that, contrary to our expectations, at ambient temperatures, the values of $\Delta G^{\#}$ for 3-aryl-DMAP[6] derivatives **7**−**10** exceed those of the corresponding 5-azaindolines.[3] Moreover, the entropies of activation for rotation ($\Delta S^{\#}$) for 5-azaindoline derivatives **5** and **6** are roughly double those of the corresponding DMAP derivatives **9** and **10**. We had expected the reverse trend due to the entropic cost of restricting rotation about the C_{Ar}−N bond in DMAP derivatives in the rate-limitng TS.

The third motivation for the computational studies was to delineate which interactions are important in restricting rotation in these systems. It was expected that this information would aid our design of configurationally stable catalyst candidates and also, given that biaryls invariably occupy equilibrium geometries wherein θ (the inter-ring dihedral angle) is $\neq$90°,[11] aid our efforts to

(8) The plateau between atropisomer peaks in the HPLC should be at least 10% of the height of the leading peak for simulation purposes. For biaryl **8**, this was not the case within the temperature range accessible using the Chiralcel OD column (max 40 °C); hence, the value of $\Delta G^{\#}$ for this derivative is a lower limit.

(9) The temperature at which $\Delta G^{\#}$ is simulated varies: **1** (20 °C), **2** (10 °C), **3** (25 °C), **7** (32 °C), and **8** (40 °C). No attempt has been made to normalize these to a common temperature. If $\Delta S^{\#}$ values for these derivatives are of magnitudes similar to those of biaryls **5** and **6**, which is likely, then such a normalization (within this limited temperature range) would not alter the values by more than 1 kJ/mol.

(10) Columns tried: Chiralcel OB, OD, and OJ and Chiralpak AD. Biaryl **4** displays an anomalous ^{1}H NMR spectrum in that both pairs of methylene protons of the pyrroline ring are almost isochronous (i.e., they appear as a pair of triplets at 250 MHz, although additional complexity is discernible at 500 MHz). All the other 5-azaindoline derivatives are clearly anisochronous and show complex splitting patterns at 250 MHz (see Supporting Information for ref 3). This presumably reflects a coincidental equivalence in the magnetic environment of these diastereotopic methylenes for this particular compound.

(11) Eliel, E. L.; Wilen, S. H. *Stereochemistry of Organic Compounds*; Wiley: New York, 1994.

(12) Slany, M.; Stang, P. J. *Synthesis* **1996**, 1019−1028 and references therein.

(13) Wolf, C.; König, W. A.; Roussel, C. *Liebigs Ann.* **1995**, 781−786.

(14) Wolf, C.; Hochmuth, D. H.; König, W. A.; Roussel, C. *Liebigs Ann.* **1996**, 357−363.

(15) Provided that racemization could be prevented during subsequent manipulations.

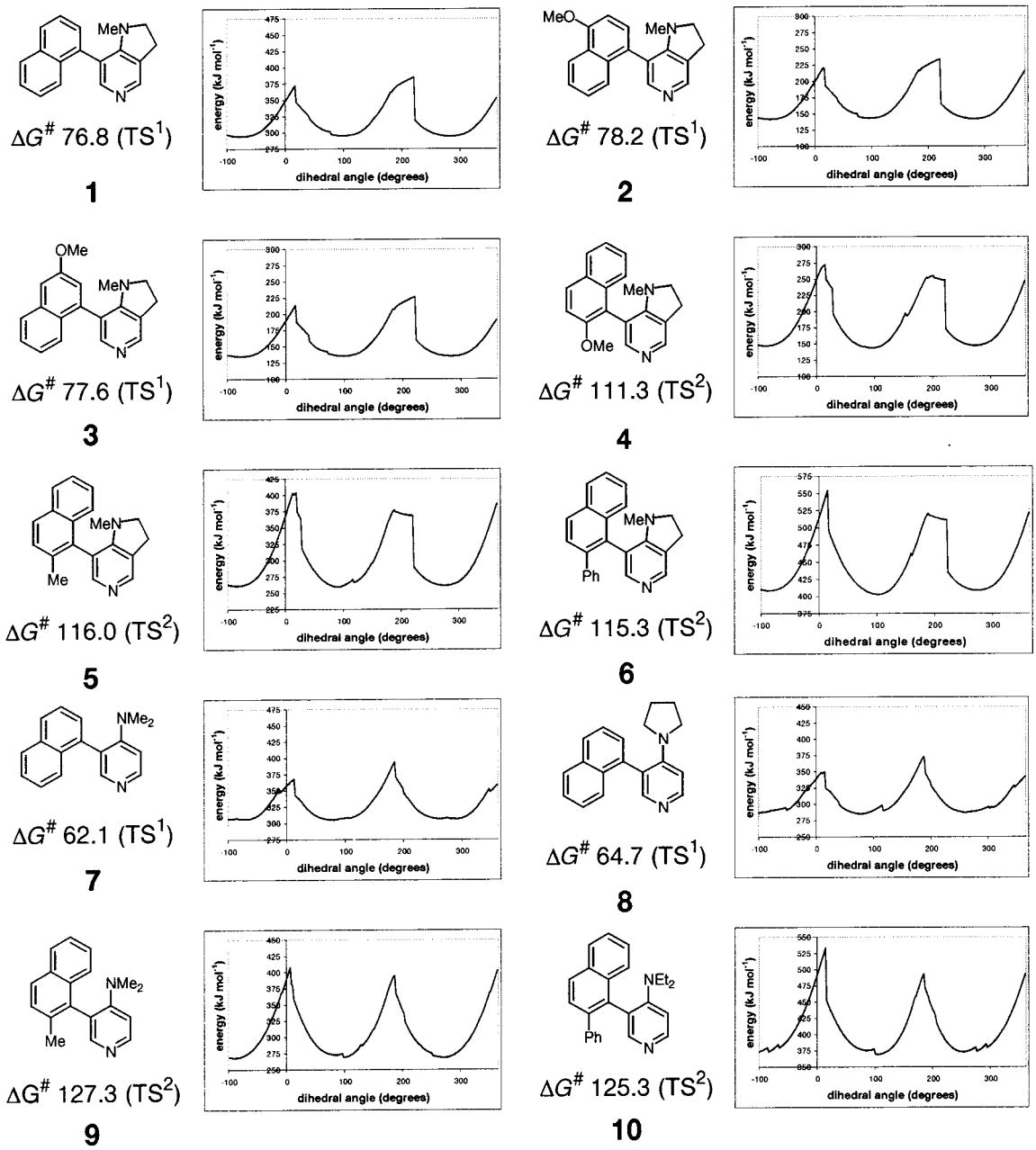

Figure 2. PM3-derived energy profiles for rotation about the biaryl axis in derivatives **1**−**10** with calculated barriers to rotation ($\Delta G^{\#}$ (kJ/mol)).

elucidate the origins of stereoinduction by these catalysts in asymmetric acylation processes.

The procedure used to generate PM3-optimized geometries for ground states (GSs) and TSs is described in Experimental Section and was applied to biaryls **1**−**10**. The free energies of enantiomerization ($\Delta G^{\#}$) generated in this way correspond to the energy required to pass over the lower of the two TSs. The $\Delta G^{\#}_{PM3}$ values are shown in Figure 2 along with the energy profiles.

The correlation between the PM3-derived $\Delta G^{\#}$ values and the experimental values across the 5-azaindoline series **1**−**6** is shown graphically in Figure 3. Although the absolute values are underestimated,[16] the relative values are in close agreement and allow an estimate of the value of $\Delta G^{\#}_{293}$ for biaryl **4** as ∼128 kJ/mol (as shown in Figure 3). This corresponds to a half-life of >10 years at ambient temperature and suggests that resolution should be feasible.

The relative broadness of the maxima corrresponding to the second transition state (at $\theta \sim 180°$, TS^2) in the 5-azaindoline series when compared to the DMAP series is due to the presence of a hydrogen bond[17] between the pyramidal pyrroline nitrogen and the naphthalene *peri*-hydrogen[18−20] (hydrogen bond lengths: **4**, 1.83 Å; **5**, 1.93 Å; **6**, 1.87 Å) near this TS. The presence of a hydrogen

(16) The PM3 rotational barriers were computed for 0 K. For the 5-azindoline series, they are ∼11% below the experimentally determined values. When corrected to 298 K using a scaling factor of 0.9761, the $\Delta G^{\#}$ values become (**1**) 89.1, (**2**) 92.1, (**3**) 90.2, (**4**) 114.6, (**5**) 123.6, and (**6**) 122.0 kJ/mol, respectively. Although the mean difference to experiment then becomes 6%, the scaled values are above and below the experimental values. For the scaling method, see: Scott, A. P.; Radom, L. *J. Phys. Chem.* **1996**, *100*, 16502−16513.

(17) Grzybowski, B. A.; Ishchenko, A. V.; DeWitte, R. S.; Whitesides, G. M.; Shakhnovich, E. I. *J. Phys. Chem. B* **2000**, *104*, 7193−7298.

(18) Afonin, A. V.; Vashchenko, A. V.; Takagi, T.; Kimura, A.; Fujiwara, H. *Can. J. Chem.* **1999**, *77*, 416−424.

(19) Park, J. K. *J. Phys. Chem. A* **2000**, *104*, 5093−5100.

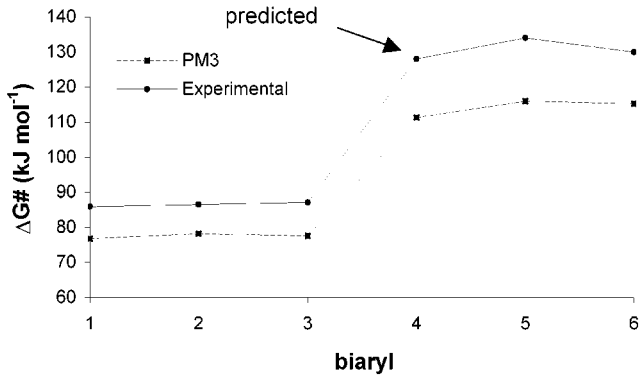

Figure 3. Correlation of experimental and PM3 values of $\Delta G^{\#}$ for 5-azaindoline derivatives **1**−**6**, showing the predicted barrier to rotation for biaryl **4** (see text).

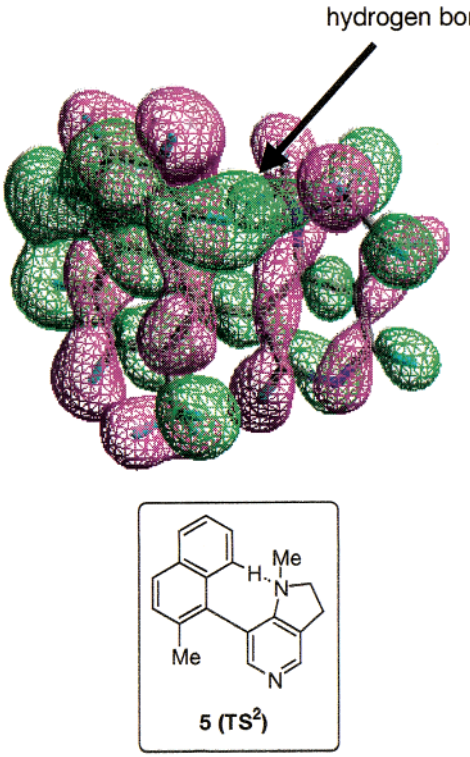

Figure 4. PM3-derived structure of TS^2 for the enantiomerization of 5-azaindoline-based biaryl **5**, showing the pyramidalization of the pyrroline nitrogen and its interaction with the naphthalene *peri*-hydrogen via a hydrogen bond (1.93 Å).

bond was verified by orbital analysis (e.g., Figure 4) and by frequency vibrations seen for these TSs using Hyperchem.[21] There is a significant lengthening of the key C−H bonds between the GS and TS^2 of biaryls **1** and **4**−**6** (Table 1). By contrast, there is no lengthening of the corresponding C−H bond between the GS and the first transition state (at $\theta \sim 0°$, TS^1) of biaryl **1** (Table 1). For 5-azaindolines **5** and **6** (Figure 2), for which TS^2 is rate limiting, this interaction accounts for the smaller values of $\Delta G^{\#}$ and $\Delta H^{\#}$ and larger values of $|\Delta S^{\#}|$ observed experimentally relative to those of DMAP derivatives **9** and **10** (Figure 2).

(20) Desiraju, G.; Steiner, T. *The Weak Hydrogen Bond: Applications to Structural Chemistry and Biology*; Oxford University Press: New York, 1999.

(21) *HyperChem* version 5.11 for Windows molecular modelling system; Hypercube, Inc.: Waterloo, Ontario, Canada, 1999.

Table 1. Changes in the PM3-Derived C−H and N···H Bond Lengths between the GS and the TS Structures of Molecules 1 (R = H), 4 (R = OMe), 5 (R = Me), and 6 (R = Ph)[a]

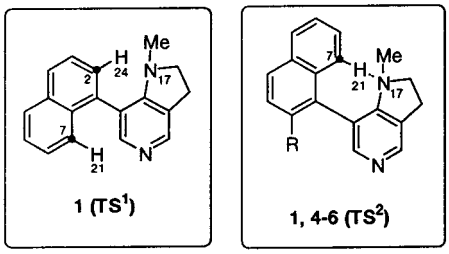

	bond		bond length (Å)
1 (R = H)	C7−H21	GS	1.097
		TS^2	1.104
	C2−H24	GS	1.096
		TS^1	1.096
	N17···H24	TS^1	2.290
	N17···H21	TS^2	1.921
4 (R = OMe)	C7−H21	GS	1.097
		TS^2	1.112
	N17···H21	TS^2	1.830
5 (R = Me)	C7−H21	GS	1.097
		TS^2	1.107
	N17···H21	TS^2	1.928
6 (R = Ph)	C7−H21	GS	1.097
		TS^2	1.110
	N17···H21	TS^2	1.873

[a] A lengthening of the C7−H21 bond length and a shortening of the N17···H21 distance between the GS and TS^2 in all cases are indicative of hydrogen bond formation.

For the non-2-substituted naphthalene derivatives **1**−**3** (Figure 2) for which the barrier corresponding to TS^1 is rate limiting, however, the PM3 calculations incorrectly predict that the 5-azaindoline series should be rotationally more stable than their DMAP analogues. This is probably because the PM3 calculations allow free rotation about the C_{Ar}−N bond in these latter structures. Ab initio calculations at the HF/STO-3G level on 3-(1-naphthyl)-DMAP **7** show that, in fact, conjugation between the dialkylamino nitrogen and the pyridine ring is maintained in TS^1 (Figures 5 and 6). The conjugation uses the p_z wave function of nitrogen and the π_z ring wave function (Tables 2 and 3). Note that the angles [$<C_{18},N_{17},C_{12} = 112.3°$, $<C_{31},N_{17},C_{12} = 112.3°$, and $<C_{18},N_{17},C_{31} = 112.0°$] show that the σ wave functions are neither purely trigonal nor purely tetrahedral but an intermediate hybridization.

The value of $\Delta G^{\#}_{HF}$ for DMAP derivative **7** is 93.7 kJ/mol, which is in reasonable agreement with the experimental value (88.6 kJ/mol). So far, we have been unable to experimentally quantify the barrier to rotation about the C_{Ar}−N bond in DMAP derivative **7** (e.g., by VT-NMR), but Fu has reported that the barrier to rotation about the C_{Ar}−N bond in his azaferrocenyl chiral DMAP derivative is ∼42 kJ/mol, which confirms that this bond can have a significant degree of double-bond character.[22] In contrast, HF calculations on 7-(1-naphthyl)-5-azaindoline **1** show that the hybridization of the pyrroline nitrogen changes significantly between the GS and TS^1 and becomes more tetrahedral (i.e., the conjugation becomes weaker). Therefore, the comparison between

(22) Hodous, B. L.; Ruble, J. C.; Fu, G. C. *J. Am. Chem. Soc.* **1999**, *121*, 2637−2638.

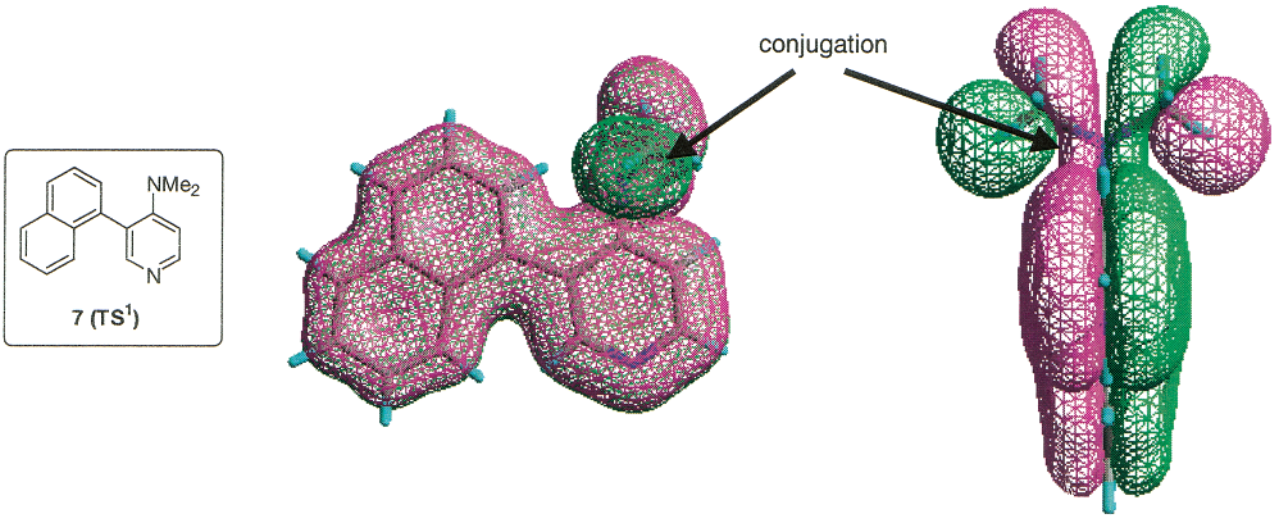

Figure 5. Molecular orbital 15 ($E = -13.58$ eV) of the HF-derived structure of TS[1] for the enantiomerization of DMAP-based biaryl **7**, showing the conjugation between the dialkylamino nitrogen and the pyridine ring.

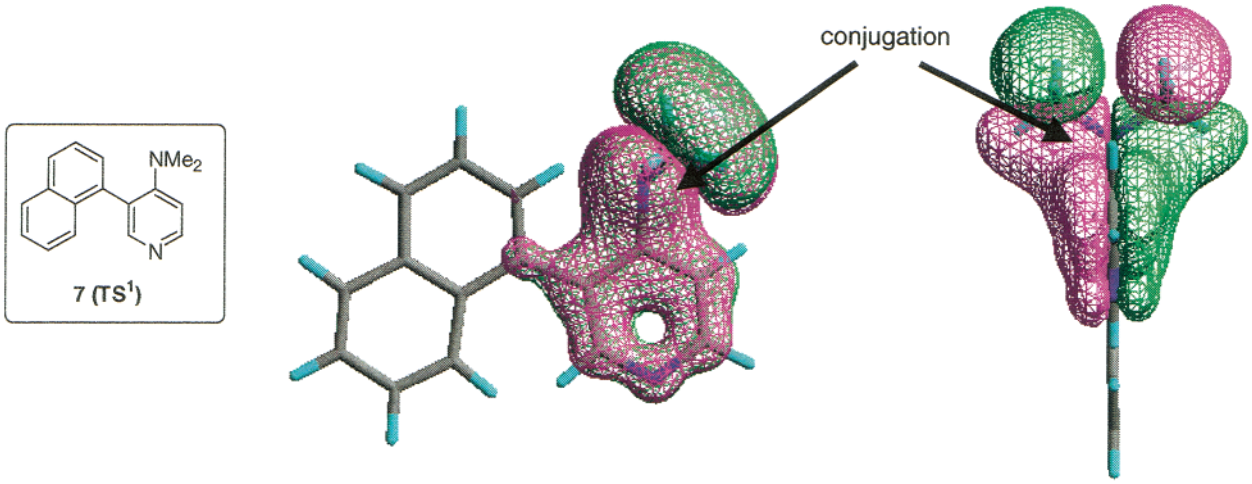

Figure 6. Molecular orbital 23 ($E = -15.67$ eV) of the HF-derived structure of TS[1] for the enantiomerization of DMAP-based biaryl **7**, showing the conjugation between the dialkylamino nitrogen and the pyridine ring.

Table 2. Coefficients of Molecular Orbital 15 ($E = -13.58$ eV) of the HF-Derived Structure of TS[1] for the Enantiomerization of DMAP-Based Biaryl 7

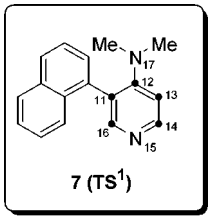

orbital 15	2*s*	2p_x	2p_y	2p_z
C11	3.22×10^{-5}	7.54×10^{-5}	-1.93×10^{-6}	2.39×10^{-1}
C12	1.20×10^{-5}	2.51×10^{-5}	1.52×10^{-4}	2.04×10^{-1}
C13	1.79×10^{-5}	-7.04×10^{-5}	-1.47×10^{-4}	1.91×10^{-1}
C14	2.90×10^{-5}	4.98×10^{-5}	1.20×10^{-4}	2.16×10^{-1}
N15	7.03×10^{-5}	-7.20×10^{-5}	-1.37×10^{-4}	2.41×10^{-1}
C16	-7.82×10^{-5}	-1.34×10^{-5}	9.12×10^{-5}	2.36×10^{-1}
N17	-7.02×10^{-5}	-1.18×10^{-4}	1.77×10^{-4}	1.02×10^{-1}

Table 3. Coefficients of Orbital 23 ($E = -15.67$ eV) of the HF-Derived Structure of TS[1] for the Enantiomerization of DMAP-Based Biaryl 7

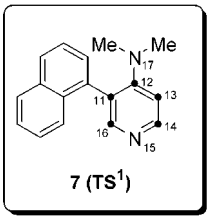

orbital 23	2*s*	2p_x	2p_y	2p_z
C11	2.48×10^{-3}	-1.20×10^{-3}	5.94×10^{-4}	-9.15×10^{-2}
C12	-3.20×10^{-3}	1.98×10^{-3}	1.58×10^{-3}	-1.78×10^{-1}
C13	6.72×10^{-4}	2.95×10^{-4}	-4.67×10^{-3}	-9.17×10^{-2}
C14	-1.42×10^{-3}	9.97×10^{-4}	8.28×10^{-4}	-5.41×10^{-2}
N15	9.34×10^{-4}	1.67×10^{-3}	6.75×10^{-4}	-4.38×10^{-2}
C16	-3.00×10^{-4}	2.99×10^{-3}	-3.24×10^{-3}	-5.44×10^{-2}
N17	8.91×10^{-4}	-4.49×10^{-4}	4.05×10^{-4}	-3.71×10^{-1}

structures given by PM3 and HF calculations for 7-(1-naphthyl)-5-azaindoline **1** and for 3-(1-naphthyl)-DMAP **7** shows that PM3 correctly predicts the rupture of conjugation between the pyrroline nitrogen and the pyridine ring for the azaindoline series, but only the HF calculations predict the conservation of conjugation between the dialkylamino nitrogen and the pyridine ring for the DMAP series (cf. Figures 7 and 8). The value

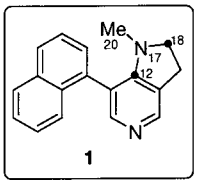

angles	*ab initio*		PM3	
	GS	TS1	GS	TS1
C20-N17-C12	118.6°	109.9°	118.2°	112.8°
C20-N17-C18	112.8°	110.7°	114.6°	111.5°
C18-N17-C12	106.7°	104.6°	107.1°	106.0°
C18-N17-C20-C12	125.8°	115.1°	127.8°	119.1°

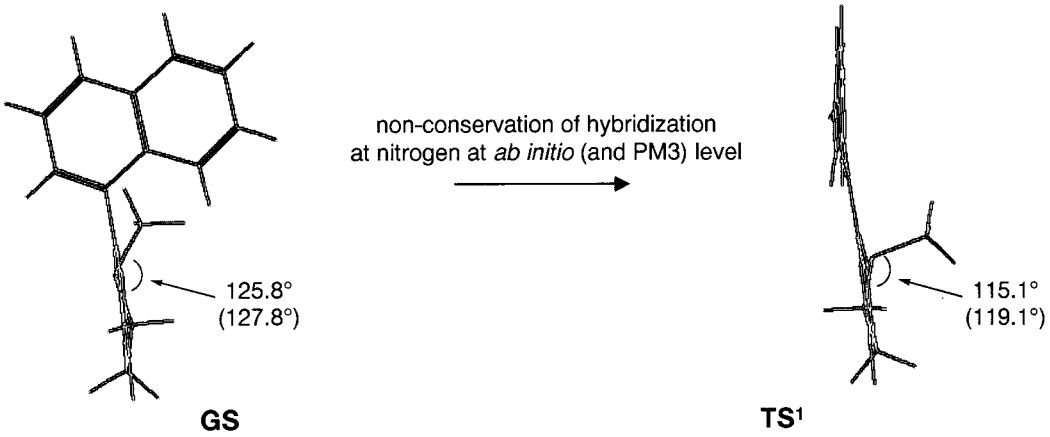

Figure 7. Comparison of the hybridization angles of 5-azaindoline-based biaryl **1** between the GS and TS[1] obtained by PM3 and HF/STO-3G calculations. Indicated dihedral angles are HF values with PM3 values in parentheses.

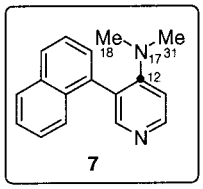

angles	*ab initio*		PM3	
	GS	TS1	GS	TS1
C31-N17-C12	112.8°	112.3°	113.1°	111.2°
C31-N17-C18	110.7°	112.0°	112.7°	112.8°
C18-N17-C12	114.8°	112.3°	115.4°	113.2°
C31-N17-C18-C12	129.2°	127.5°	132.0°	127.4°

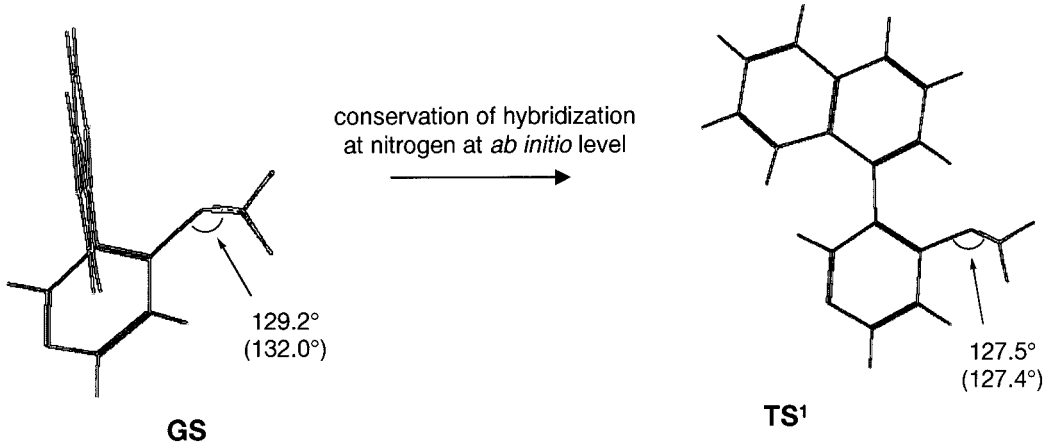

Figure 8. Comparison of the hybridization angles of DMAP-based biaryl **7** between the GS and TS[1] obtained by PM3 and HF/STO-3G calculations. Indicated dihedral angles are HF values with PM3 values in parentheses.

of $\Delta G^{\#}_{HF}$ for 5-azaindoline derivative **1** is 83.0 kJ/mol, which is in good agreement with the experimental value (85.9 kJ/mol).

DMAP derivative **7** and 5-azaindoline derivative **1** have also been compared by DFT/B3LYP/6-31G* calculations. The *geometries* obtained using the DFT calculations, like the HF calculations, show a conservation of the conjugation between the GS and TS[1] for 3-(1-naphthyl)-DMAP **7** (Figures S9 and S10 and Tables S4 and S5, Supporting Information) and a rupture of the conjugation for the 5-azaindoline analogue **1**. However, the DFT-derived *energies* do not reflect the experimental situation so closely [$\Delta G^{\#}_{DFT}$ (**7**) = 80.0 kJ/mol and $\Delta G^{\#}_{DFT}$ (**1**) = 81.3 kJ/mol].

Conclusions

PM3 calculations of the barriers to rotation of a series of atropisomeric 7-(1-naphthyl)-5-azaindolines **1**−**6** and 3-(1-naphthyl)-DMAPs **7**−**10** have been performed. These calculations revealed that, in both series, TS[1] ($\theta \sim 0°$) is rate limiting for configurationally labile derivatives (**1**−**3**, **7**, and **8**) and that TS[2] ($\theta \sim 180°$) is rate limiting for configurationally stable derivatives (**4**−**6**, **9**, and **10**). Consideration of the lower TS energy in each case has allowed the estimation of relative barriers to enantiomerization as a function of naphthyl substitution across each series. For the 5-azaindolines, the correlation between the barriers to rotation generated by PM3 and the

experimental barriers was good, although the absolute values were consistently underestimated.[16] Previous studies have also shown that semiempirical methods tend to underestimate rotational barriers in similar atropisomeric systems,[23,24] a phenomenon that may be the result of a systematic error in the PM3 parameterization[25] or may arise because the calculations are performed for the gas phase.[26,27] The PM3 calculations also revealed that for configurationally stable derivatives (**4**−**6**), the barrier to enantiomerization (TS^2) is lower in energy relative to that of the DMAP series (**9** and **10**) due to the presence of a hydrogen bond between the pyramidal ($\sim sp^3$) pyrroline nitrogen and the naphthalene *peri*-hydrogen. For the DMAPs, correlation of PM3 vs experimental barriers was less satisfactory because the PM3 calculations failed to predict that, for configurationally labile derivatives (**7** and **8**), the barrier to enantiomerization (TS^1) is also lower in energy than that for the corresponding 5-azaindolines **1**−**3**. However, HF/STO-3G and DFT/B3LYP/6-31G* calculations suggest that this is because the PM3 calculations fail to allow the dialkylamino nitrogen to remain significantly planarized ($\sim sp^2$) in TS^1. This planarity raises the energy of the DMAP TS^1 relative to that of the corresponding 5-azaindoline TS^1 in which the pyrroline nitrogen remains more pyramidal. The magnitude of this difference in rotational barriers is more accurately predicted by the HF calculations than by the DFT calculations (cf. experimental values) presumably due to the limitations of the exchange and correlation functionals used in DFT, where self-interaction is essential to give good fit to experimental results.[28]

Rotational energy barriers in biaryls reflect the difference in energy between the GS and the rate-limiting TS. The most significant factors determining this energy difference are the destabilization of the TS by steric effects of *ortho* substituents (enhanced by the butressing effects of *meta* substituents) and the stabilization of the TS (to a greater or lesser extent depending on the electronic influence of substituents) by $\pi-\pi$ conjugation across the biaryl bond.[29] A number of additional factors have also been proposed to be important, particularly for functionalized biaryls and heterobiaryls.[30] For example, solvent-dependent field effects, dipole−dipole electrostatic interactions, and CH−π interactions have been proposed in certain instances.[13,14,31] The stabilization of the TSs by weak CH···N hydrogen bonds has also been proposed previously[32,33] but not substantiated. Our studies indicate that this type of attractive interaction in rate-limiting TSs can have a significant influence on rotational barriers. The importance of this interaction appears to be closely dependent on the hybridization state of the acceptor nitrogen atom and is manifested particularly in the magnitude of the activation entropy term $|\Delta S^{\#}|$ (cf. 5-azaindoline-based biaryls **5** and **6**, $\Delta S^{\#} = -106$ and -81 J mol^{-1} K^{-1}, respectively, vs DMAP-based biaryls **9** and **10**, $\Delta S^{\#} = -63$ and -37 J mol^{-1} K^{-1}, respectively). It appears therefore that the orbital ordering associated with hydrogen bond formation, although entropically costly, is sufficiently enthalpically favorable that, together, these terms reduce the configurational stablity of 5-azaindolines relative to that of analogous DMAPs at ambient temperatures (i.e., they lower $\Delta G^{\#}$). It is also interesting that the hybridization state of nitrogen also influences the energies of the TSs for which no CH···N hydrogen bonding occurs (i.e., for biaryls **1**−**3**, **7**, and **8**). UV, single-crystal X-ray, and other data confirm that 4-aminopyridines (including DMAPs and 5-azaindolines) have significant conjugation across their C_{Ar}−N bonds and, consequently, have significantly planarized dialkylamino nitrogen atoms in the GS.[22,34,35] The loss of this conjugation in the rate-limiting TS for 5-azaindoline-based biaryl rotation, but not for the DMAP-based biaryl, is predicted by the ab initio HF/STO-3G and the DFT/B3LYP/6-31G* calculations. Both methods give very similar geometries to the TSs, but the HF model, even at the STO-3G level of theory, more accurately reflects the experimental energies than the DFT, which, like the PM3 calculations, appears to underestimate the activation energies.[24] We have previously speculated[3] that the lower barriers to rotation found experimentally for configurationally labile 5-azaindoline-based biaryls relative to those of analogous DMAPs might be attributed to the concept of Baeyer (angle) strain.[11] Hence, for 5-azaindoline-based biaryls, the shift in hybridization of the pyrroline nitrogen toward sp^3 that allows bending of the C_{Ar}−N bond away from the biaryl axis (and hence lowering the TS energy, $\Delta G^{\#}$) is facilitated by the concomitant relief of angle strain within the five-membered ring. The HF and DFT results would appear to provide support for this qualitative interpretation.

On a practical level, our studies have allowed prediction of the barriers to rotation for compounds that are potential catalysts and provided a rationale for the apparently anomolous barriers to racemization of 5-azaindolines relative to those of DMAPs. Moreover, these studies have provided important insight into the electronic characteristics of these molecules that should aid our emerging understanding of the origins of stereoinduction by these molecules when employed as catalysts in asymmetric processes.

Experimental Section

Compound Synthesis and Data Collection for Eyring Plots. The syntheses of compounds **1**−**9**[3] and **11**[4] have been described previously. Racemization studies on compounds **5**, **6**, **9**, and **10**, which were resolved using semiprep enantioselective HPLC as described previously,[3,4] were performed on ~3 mg samples in freshly distilled benzene (2 mL) in sealed Wheaton vials (3.0 mL V-vials with solid screw caps) suspended in a thermostated silicone oil bath (stable to ±1 °C) equipped with a stirrer. Aliquots of 10 μL were removed

(23) Zoltewicz, J. A.; Maier, N. M.; Fabian, W. M. F. *J. Org. Chem.* **1997**, *62*, 2763−2766.
(24) Cross, W.; Hawkes, G. E.; Kroemer, R. T.; Liedl, K. R.; Loerting, T.; Nasser, R.; Pritchard, R. G.; Steele, M.; Watkinson, M.; Whiting, A. *J. Chem. Soc., Perkin Trans. 2* **2001**, 459−467.
(25) Bringmann, G.; Vitt, D.; Kraus, J.; Breuning, M. *Tetrahedron* **1998**, *54*, 10691−10698.
(26) Lomas, J. S.; Adenier, A.; Cordier, C.; Lacroix, J.-C. *J. Chem. Soc., Perkin Trans. 2* **1998**, 2647−2652.
(27) Seiner, T.; Holzgrabe, U.; Drosihn, S.; Brandt, W. *J. Chem. Soc., Perkin Trans. 2* **1999**, 1827−1834.
(28) (a) Tseng, T. J.; Whitehead, M. A. *Phys. Rev. A* **1981**, *24*, 16−20. (b) Tseng, T. J.; Whitehead, M. A. *Phys. Rev. A* **1981**, *24*, 21−28. (c) Kurita, N.; Tanaka, S.; Itoh, S. *J. Phys. Chem. A* **2000**, *104*, 8114−8120. (d) Patchkovskii, S.; Autschbach, J.; Ziegler, T. *J. Chem. Phys.* **2001**, *115*, 26−42.
(29) Westheimer, F. H. *Calculation of the Magnitude of Steric Effects*; Wiley: New York, 1956.
(30) Gallo, R.; Roussel, C.; Berg, U. *Adv. Heterocycl. Chem.* **1988**, *43*, 173−299.
(31) Zoltewicz, J. A.; Maier, N. M. *J. Org. Chem.* **1998**, *63*, 4985−4990 and references therein.
(32) See: ref 30, p 259.
(33) Barone, V.; Lelj, F.; Russo, N. *Int. J. Quantum Chem.* **1986**, *29*, 541−551.
(34) Batts, B. D.; Spinner, E. *Aust. J. Chem.* **1969**, *22*, 2595−2610.
(35) Batts, B. D.; Spinner, E. *Aust. J. Chem.* **1969**, *22*, 2611−2626.

at appropriate time intervals, and the enantiomeric excess was determined by area/area integration of the analytical enantioselective HPLC chromatogram. Kinetic parameters for racemization[1] and enantiomerization[1] were obtained from Eyring plots (see Supporting Information).[36−38]

Dynamic HPLC and Chromatogram Simulation. Dynamic enantioselective HPLC[39] was performed on a Hewlett-Packard HP1100 system equipped with a thermostatic column compartment (Peltier type, HP G1316A, stable to ±0.15 °C). Elution profiles were obtained following the injection of ∼5 μg of biaryl with UV detection at 250 nm under conditions detailed in the Supporting Information.

The rate constant of enantiomerization (k_{enant}) and, hence, the free energy of activation for rotation ($\Delta G^{\#}$) were determined by computer simulation of the HPLC elution profiles employing the program package Mimesis 1.5.[40] The computer simulation is based on the discontinuous plate model applicable to partition processes, which was first used by Schurig for the simulation of dynamic chromatograms (program SIMUL).[41−45] The program package employed here has been used previously for the rapid determination of rotational energy barriers in axially chiral biphenyls (dynamic GC and HPLC),[13,14] lignans (dynamic SFC),[46] planar-chiral dioxa[*n*]paracyclophanes,[47] and [*n*]paracyclophanes (dynamic GC).[48] The program requires the input of a theoretical plate number (obtained experimentally), mobile-phase dead time, and retention times. The error of determination of the energy barrier to enantiomerization is estimated to be less than 0.5 kJ/mol, with the major contribution being due to the thermostatization and temperature measurement and a contribution of approximately 0.2 kJ/mol due to the simulation approximation algorithm. The reproducibility is better than 0.3 kJ/mol within the same experimental system. The energy barriers are valid for the given chromatographic environment, usually exhibit a weak dependency on both the solvent and the optically active stationary phase, and thus might differ slightly from theoretical values of single molecules in the gas phase.

Calculations. All PM3, HF/STO-3G, and DFT/B3LYP/6-31G* calculations were performed using the Gaussian 98 package on a PC.[49,50] Inputs for the starting structure of the semiempirical calculations on each molecule were created by drawing the structures in the HyperChem[21] visualizer. PM3[51] geometry optimization was performed in each calculation, and the optimizations were carried out in internal coordinates.[52] Energy scans[53] were performed at the PM3 level around the biaryl axis ($\theta = 0-360°$) in 2° intervals, followed by optimization at the PM3, HF/STO-3G, or DFT/B3LYP/6-31G* level of the structures corresponding to the two energy maxima (TS^1 and TS^2 in Figure 2)[54] and the two degenerate energy minima (the enantiomeric GSs) by the PM3 method. The energy scans optimize each structure initially with a fixed dihedral angle; minima and maxima are reoptimized without constraining the dihedral angle. The optimized structures of the minima then correspond to the enantiomers. The optimization for the TS (the saddle point of the potential energy surface) is different from that used to find the GS structure minima of the potential energy surface. To optimize a local minimum, the Berny optimization[55] was applied; this uses a combination of rational function optimization and linear search steps. The algorithm for the TS optimization first computes the Hessian[56] matrix and then moves the nuclei to increase the energy in the directions corresponding to the negative values of the Hessian and of the negative eigenvalue and to minimize the energy in the directions of positive values of the Hessian. A TS is a first-order saddle point with only one imaginary frequency.[57] To verify that this TS corresponds to the enantiomerization, a frequency analysis was performed and the imaginary frequency corresponding to a rotation around the dihedral angle θ was animated using HyperChem.[21] All quantum mechanical calculations used RHF wave functions.

Acknowledgment. The generous financial support of this work by the Leverhulme Trust, GlaxoSmithKline, the EPSRC, and the NSERC (Canada) is gratefully acknowledged. We thank Mr. Jan-Philip Plog (University of Hamburg) for performing the racemization experiments on biaryl **10**.

Supporting Information Available: Experimental and simulated enantioselective HPLC chromatograms (elution profiles) for biaryls **1**−**3**, **7**, and **8**, Eyring plots and data points for the racemization of biaryls **5**, **6**, **9**, and **10**, coordinates and computed total energies for PM3, HF, and DFT calculations on biaryls **1**−**10**, and Figures S9 and S10 and Tables S4 and S5 (DFT MOs 12 and 25 for TS^1 of biaryl **7**). This material is available free of charge via the Internet at http://pubs.acs.org.

JO015593Q

(36) Cagle, F. W.; Eyring, H. *J. Am. Chem. Soc.* **1951**, *73*, 5628−5630.
(37) Hall, D. M.; Harris, M. M. *J. Chem. Soc.* **1960**, 490−494.
(38) Cooke, A. S.; Harris, M. M. *J. Chem. Soc. C* **1967**, 988−992.
(39) Veciana, J.; Crespo, M. I. *Angew. Chem., Int. Ed. Engl.* **1991**, *30*, 74−76.
(40) Hochmuth, D. H. *Mimesis 1.5* program package optimized for high-performance parallel processsing on a Silicon Graphics PowerChallenge SC900 or the parallel computing system Hewlett-Packard V-Class Enterprise server V2250 (PA-8200 processor); *Mimesis 2.1 for Windows 95* (PC-compatible computers) for smaller simulations; University of Hamburg: Hamburg, Germany, 1995−1999.
(41) Schurig, V.; Jung, M.; Schleimer, M.; Klärner, F.-G. *Chem. Ber.* **1992**, *125*, 1301−1303.
(42) Jung, M.; Schurig, V. *J. Am. Chem. Soc.* **1992**, *114*, 529−534.
(43) Jung, M.; Fluck, M.; Schurig, V. *Chirality* **1994**, *6*, 510−512.
(44) Jung, M. *QCPE Bull.* **1992**, *12*, 52.
(45) Trapp, O.; Schurig, V. *J. Am. Chem. Soc.* **2000**, *122*, 1424−1430.
(46) Wolf, C.; Pirkle, W. H.; Welch, C. J.; Hochmuth, D. H.; König, W. A.; Chee, G.-L.; Charlton, J. L. *J. Org. Chem.* **1997**, *62*, 5208−5210.
(47) Hochmuth, D. H.; König, W. A. *Liebigs Ann.* **1996**, 947−951.
(48) Hochmuth, D. H.; König, W. A. *Tetrahedron: Asymmetry* **1999**, *10*, 1089−1097.
(49) Schmidt, M. W.; Baldridge, K. K.; Botz, J. A.; Hensen, J. H.; Koseki, S.; Gorden, M. S.; Nguyen, K. A.; Windus, T. L.; Elbert, S. T. *QCPE Bull.* **1990**, *10*, 52.
(50) Schmidt, M. W.; Baldridge, K. K.; Botz, J. A.; Elbert, S. T.; Gorden, M. S.; Hensen, J. H.; Koseki, S.; Matsununga, N.; Nguyen, K. A.; Su, S.; Windus, T. L.; Dupuis, M.; Montgomery, J. A. *J. Comput. Chem.* **1993**, *14*, 1347.
(51) Stewart, J. J. P. *J. Comput. Chem.* **1989**, *10*, 209−220.
(52) Frisch, M. J.; Trucks, G. W.; Schlegel, H. B.; Scuseria, G. E.; Robb, M. A.; Cheeseman, J. R.; Zakrzewski, V. G.; Montgomery, J. A., Jr.; Stratmann, R. E.; Burant, J. C.; Dapprich, S.; Millam, J. M.; Daniels, A. D.; Kudin, K. N.; Strain, M. C.; Farkas, O.; Tomasi, J.; Barone, V.; Cossi, M.; Cammi, R.; Mennucci, B.; Pomelli, C.; Adamo, C.; Clifford, S.; Ochterski, J.; Petersson, G. A.; Ayala, P. Y.; Cui, Q.; Morokuma, K.; Malick, D. K.; Rabuck, A. D.; Raghavachari, K.; Foresman, J. B.; Cioslowski, J.; Ortiz, J. V.; Stefanov, B. B.; Liu, G.; Liashenko, A.; Piskorz, P.; Komaromi, I.; Gomperts, R.; Martin, R. L.; Fox, D. J.; Keith, T.; Al-Laham, M. A.; Peng, C. Y.; Nanayakkara, A.; Gonzalez, C.; Challacombe, M.; Gill, P. M. W.; Johnson, B. G.; Chen, W.; Wong, M. W.; Andres, J. L.; Head-Gordon, M.; Replogle, E. S.; Pople, J. A. *Gaussian 98*, revision A.5; Gaussian, Inc.: Pittsburgh, PA, 1998.
(53) Nezel, T.; Muller-Plathe, F.; Muller, M. D.; Buser, H.-R. *Chemosphere* **1997**, *35*, 1895−1906.
(54) For all calculations, 0° corresponds to the situation where both aryl rings are coplanar and the biaryl bond is *s-cis* with respect to the pyridine nitrogen and the naphthalene framework.
(55) Schlegel, H. B. *J. Comput. Chem.* **1982**, *3*, 214.
(56) Peng, C.; Ayala, P. Y.; Schlegel, H. B.; Frisch, M. J. *J. Comput. Chem.* **1996**, *17*, 49.
(57) Foresman, J. B.; Frisch, A. *Exploring Chemistry with Electronic Structure Methods*, 2nd ed.; Gaussian, Inc.: Pittsburgh, PA, 1996.